An NMR-Guided High Temperature Electrolyte Design Using a Novel PF_5 Marker

Noah M. Johnson and Zhengcheng Zhang*

[1]Chemical Sciences and Engineering Division

Argonne National Laboratory

9700 S. Cass Ave., Lemont, IL 60439, USA

Email: zzhang@anl.gov

Abstract

The thermal degradation of electrolytes containing lithium hexafluorophosphate ($LiPF_6$) is well-studied subject. However, practical application of the knowledge is difficult since the effects of the degradation process on battery performance are not well-known. Here we propose a novel NMR experimental setup allowing direct observation of the effects of various perturbations on the electrolyte thermal degradation process, which guides the design and synthesis of new additives that improve lithium-ion battery performance at elevated temperatures.

1. Introduction

Lithium-ion batteries (LIBs) are the most widely used energy storage technology in the world, and researchers are constantly striving to improve their capacity, energy density, safety, and longevity to broaden their applications. One problem in the most common systems is thermal stability, where electrolytes containing $LiPF_6$ will rapidly degrade at elevated temperatures.[1] Much work has been done in trying to enable high temperature operation,

including changing the lithium salt[2-5], using different electrolyte solvents[6], or using electrolyte additives to stabilize the interface or the bulk of the electrolyte[7-18].

The commonly accepted mechanism for electrolyte decomposition at high temperatures was initially proposed by Campion *et al.*[19-20], which involves pentafluorophosphorous (PF_5) reacting with trace amount of protic impurities to form trifluorophosphorous oxide (POF_3), which can then react *via* an autocatalytic mechanism to generate carbon dioxide (CO_2), fluoroalkyl chains, and an extra equivalent of POF_3.

Later research[21-22] demonstrated that minor perturbations, such as the nature of the container, could influence this reaction. Their results matched those of Campion when glass surfaces were present, but polymer containers generated no visible POF_3, and indeed showed little to no signs of degradation at all. Later studies proposed two separate reaction mechanisms[23], where the presence of water is the main determining factor, and when water concentration is kept consistently low[22, 24] the concentration of degradation products is difficult to detect. However, all proposed mechanisms agree that the starting point for degradation is the generation of PF_5.

Nuclear magnetic resonance spectroscopy (NMR) is a quantitative, non-destructive, and *in-situ* technique, making it well-suited for the study of long-term processes like electrolyte degradation. However, it suffers from low sensitivity and dynamic range, which limits its use in a well-controlled experiment. NMR has been exploited in the study of electrolyte

degradation before, analyzing the effect of protic impurities,[21] additives[7, 13], or the overall mechanism[20]. However, while PF_5 is broadly agreed to be the starting point for thermal degradation, it has not been directly detected by NMR in electrolyte solutions. In this work, a novel experimental setup was proposed to observe the generation of PF_5 over time, therefore allowing us to study the effects of different perturbations on the degradation process. Using this information, electrolyte additives that can limit the reactivity or generation of PF_5 was designed, synthesized, and electrochemically tested in a lithium-ion cell with improved overall battery performance.

2. Methods

2.1 NMR measurements. Samples for NMR spectroscopy were prepared in an argon-filled glovebox. All glassware was dried at 120°C overnight and immediately transferred to the glovebox. PTFE/FEP inserts were dried overnight at 50°C and immediately transferred to the glovebox. Battery-grade Gen 2 electrolyte, consisting of 1.2 M $LiPF_6$ in a mixture of ethylene carbonate (EC) and ethyl methyl carbonate (EMC) (3:7 w/w) was provided by Tomiyama Pure Chemical Industries. Deuterated solvents were obtained from Cambridge Isotopes and used as received. NMC622 powder was dried under vacuum at 130°C overnight. The chemical delithiation was carried out following a literature reported procedure[25] by reacting NMC622 powers with an equivalent of nitronium tetrafluoroborate (NO_2BF_4) as reported in literature using dried, distilled, and degassed acetonitrile (with a water content < 20 ppm) as reaction solvent.

NMR spectra were taken on a Bruker Ultrashield 300 MHz equipped with a Broadband Observe (BBO) probe. ^{1}H NMR spectra were referenced to the EC singlet at 4.510 ppm, ^{19}F spectra to the $LiPF_6$ doublet at -74.0 ppm, and ^{31}P spectra to the $LiPF_6$ septet at -145.0 ppm. All spectra of the electrolyte samples were taken at 298K after exposed to high temperatures for various durations.

2.2 Electrode materials and cell testing. Electrochemical testing was performed on a MACCOR Series 4000 Automated Test System. 2032-coin cells were assembled using electrodes made by the Cell Analysis, Modeling, and Prototyping (CAMP) facility at Argonne National Laboratory. The cathode was made of 90 wt% $Li(Ni_{0.6}Mn_{0.2}Co_{0.2})O_2$ (NMC622, EcoPro), with 5 wt% C45 carbon black (Timcal) and 5% PVDF binder (Solvey 5130) on a 20 μm aluminum current collector. The total active material loading was 9.0 mg/cm^2. The anode was composed of ~92 wt% graphite (Superior Graphite SLC1506T), with 2 wt% C45, and 6 wt% PVDF (Kureha 9300) on a 10 μm copper current collector. The graphite loading was 5.9 mg/cm^2. The electrodes were dried under vacuum at 130°C overnight before use. All cells contained Celgard 2325 separators and were filled with 40 μL of electrolyte. Cells were initially cycled at room temperature at a C/20 rate between 2.7 and 4.2 V for three cycles and were then brought to a 55°C oven where they were formed between 2.7 and 4.2 V at C/10 rate, with a 4.2 V constant voltage hold. They were then cycled at 1 C rate for 100 cycles, including a hybrid pulse power characterization (HPPC) sequence every 25 cycles. All electrochemical results shown are an average of two cells.

2.3 Organic synthesis.

Phosphonitrilic chloride trimer was recrystallized in hexane and sublimed prior to use. All other solvents and reagents were used as received.

*2.3.1 Hexa(2,2,2-trifluoroethoxy)cyclotriphosphazene (**PzTFE**).* 775 mg (32 mmol) of sodium metal was washed with pentane and placed in a dry round-bottom flask. A nitrogen atmosphere was established, 40 mL of dry ethyl ether was added via syringe, and the temperature was brought down to 2°C using an ice bath. 4.475 g (45 mmol) of 2,2,2-trifluoroethanol was slowly added via syringe, maintaining an internal temperature below 10°C. Once addition was complete, the flask was allowed to warm to room temperature, and was stirred for 1 hour. Subsequently, the flask was again cooled, and a solution of 657 mg (1.9 mmol) phosphonitrilic chloride trimer in diethyl ether was added *via* syringe. The reaction was stirred at room temperature overnight. The solution was washed with water and evaporated to yield a white, waxy solid. This was recrystallized in hexanes to yield 735 mg (53% yield) of a white, crystalline solid. ^{1}H NMR (300 MHz, *chloroform-d*) δ 4.36 – 4.20 (m, 1H), ^{13}C[^{1}H] NMR (75 MHz, Chloroform-d) δ 122.31 (qdd, J = 277.3, 7.4, 3.8 Hz), 63.05 (qd, J = 38.4, 2.9 Hz). ^{19}F NMR (282 MHz, *chloroform-d*) δ -75.21 (t, J = 7.9 Hz), ^{31}P[^{1}H] NMR (121 MHz, *chloroform-d*) δ 16.86 (s).

*2.3.2 Hexa(2,2,3,3-tetrafluoro-1-propoxy)cyclotriphosphazene (**PzTFP**).* The procedure was carried out same as PzTFE using 524 mg (22 mmol) of sodium metal, 4.017 g (30 mmol) of 2,2,3,3-tetrafluoro-1-propanol, and 671 mg (1.9 mmol) of phosphonitrilic chloride trimer. The product was purified by sublimation at 120°C to yield 631 mg (38% yield) of a waxy solid.

^{1}H NMR (300 MHz, *chloroform-d*) δ 5.89 (tt, J = 53.0, 3.7 Hz, 1H), 4.70 – 3.89 (m, 1H). ^{13}C[^{1}H] NMR (75 MHz, *acetone-d6*) δ 109.27 (tt, J = 248.6, 35.2 Hz), 108.97 (tt, J = 250.0, 36.2 Hz), 62.32 (td, J = 30.2, 1.2 Hz). ^{19}F NMR (282 MHz, *chloroform-d*) δ -124.63 (td, J = 12.4, 3.1 Hz), -137.92 (d, J = 53.0 Hz). ^{31}P[^{1}H] NMR (121 MHz, *chloroform-d*) δ 17.08 (s).

*2.3.3 Hexa(1,1,1,3,3,3-hexafluoro-2-propoxy)cyclotriphosphazene (**PzHFiP**).* The procedure was carried out same as PzTFE using 460 mg (19 mmol) sodium metal, 3.392 g 1,1,1,3,3,3-hexafluoro-2-propanol (20 mmol), and 715 mg (1.9 mmol) phosphonitrilic chloride trimer. The product was purified by sublimation to yield 470 mg (22% yield) of an off-white solid. ^{1}H NMR (300 MHz, *acetone-d6*) δ 5.98 – 5.69 (m, 1H). ^{13}C[^{1}H] NMR (75 MHz, Acetone-d6) δ 120.15 (q, J = 282.1, 280.4 Hz), 71.48 (hept, J = 35.9, 34.9 Hz).. ^{19}F NMR (282 MHz, Acetone-d6) δ -74.27 (d, J = 4.8 Hz). ^{31}P[^{1}H] NMR (121 MHz, *acetone-d6*) δ 15.09 (s).

3. Results and Discussion

3.1 Discovery and characterization of new PF_5 complex

The commonly accepted mechanism for electrolyte decomposition at high temperatures was initially proposed by Campion *et al.*[19-20], which involves PF_5 reacting with trace protic impurities to form POF_3, which can then react *via* an autocatalytic mechanism to generate CO_2, fluoroalkyl chains, and an extra equivalent of POF_3. To study the dynamic structure and chemical composition of the electrolyte at elevated temperatures, a new NMR setup was established as shown in **Figure 1**. An PTFE/FPE insert design could eliminate the complication of the deuterated solvent with the subject testing electrolyte affording a more

accurate information.

Testing temperatures of 50°C and 80°C were selected to represent medium and extreme temperatures for lithium-ion battery operation. When a sample of Gen 2 electrolyte was exposed to such a high temperature for an extended period in our new experimental setup, a new set of peaks was seen in both ^{19}F and ^{31}P spectra as shown in **Figure 2**. This consisted of a doublet of doublets (-63.70 ppm, J= 766.9, 56.9 Hz) and a doublet of quintets (-80.84 ppm, J = 743.5 Hz, 57.0 Hz). Coincident to this was the growth of a doublet of quintets in the ^{31}P NMR (-143.0 ppm, J = 765.0, 745.0 Hz). Both ^{19}F and ^{31}P-NMR indicates the existence of a complex of PF_5 with a Lewis base. However, attempts to positively identify this complex have so far failed.

As it is widely accepted that the decomposition mechanism of Gen 2 electrolyte begins with the formation of PF_5, the potential to use this PF_5-base complex as a marker for electrolyte decomposition was explored by NMR. Many additives have been tested for the purpose of suppressing this process and improving the cell performance at high temperatures, with one of the most common one being *N,N*-dimethylacetamide (DMAc)[15]. In order to test our hypothesis, 2% DMAc (w/w) was chosen and added to Gen 2 electrolyte with the belief that this would limit the growth of this signal. The ^{19}F-NMR spectra shown in **Figure 3a** indicate the strong coordination of PF_5 with DMAc, based on the appearance of a second set of peaks indicative of a separate PF_5 complex being formed. The overall strength of the new PF_5 signal was restricted when compared to the unmodified electrolyte (**Figure 3b**), indicating that the

concentration was limited as well.

Validated by the DMAc experiment, we started to test different perturbations to the electrolyte system to investigate their effects on the thermal degradation process. **Figure 4** shows the addition of different materials to Gen 2 electrolyte aged for elongated period of times at both 50°C and 80°C. It is manifest that addition of the cathode active material NMC622 actually increased the decomposition rate over the baseline electrolyte when treated at the same temperature. This could be due to the addition of a catalytic surface, or potentially the dissolution of the transition metal ions into the electrolyte solution. Water prevented any complex from forming, potentially because of the rapid reaction of PF_5 with H_2O.

One piece of evidence supporting the role of transition metals in the decomposition process is the changing peak width in electrolyte solution. While peak width is dependent on many factors, such as ionic strength, rotational averaging, 90° pulse calibration, or the quality of the magnetic shimming, it can also be affected by the addition of paramagnetic ions. As Mn^{2+} is a paramagnetic species, it is expected to see peak broadening as its concentration increased in the solution. This explains the significant peak broadening for difluorophosphate for the NMC sample as evidenced by the NMR data shown in **Figure 5**. Hexafluorophosphate $PF6^-$ maintained a constant peak width, which indicates a close association between Mn^{2+} and difluorophosphate. An alternative explanation is an increase in water content leading to higher rotational averaging, however the same degree of peak broadening wasn't seen in a sample with added H_2O.

Owing to the chemical composition and morphology change of the cathode material during repeated lithiation and delithiation, the reactivity of the electrolyte with cathode at different state of charge (SOC) could be differing. Given pristine NMC622 sample is considered as 100% discharged stage, a chemical delithiation process[25] was employed to prepare an approximately 50% SOC NMC622 cathode. Surprisingly, the delithiated NMC622 sample didn't significantly affect the electrolyte decomposition process under this testing condition, which supports the theory of transition metal dissolution (**Figure 6**).

3.2 Design of advanced high-temperature electrolytes

Now that a working system was established, we undertook to use the information to design an electrolyte that could perform well at elevated temperatures. As DMAc is well understood to be effective for these purposes, we sought an alternative whose mechanism and effectiveness is less well studied. One class of compounds that has been shown to slow the decomposition of electrolyte are the cyclic phosphazenes[10], although there is considerable disagreement as to their mechanism of action[6, 10, 13, 26-27]. In order to validate the electrochemical performance of this type of additives, a series of fluorinated phosphazenes were designed. Three substituted phosphazenes were synthesized and their chemical structure and purity were identified by NMR, FT-IR and GC-MS. When 2% hexa(trifluoroethoxy)cyclotriphosphazene[26] was added to Gen 2 electrolyte, the growth of the new PF_5-base marker was restricted, similarly to DMAc (**Figure 7a**). To validate the NMR results, the lithium-ion battery was assembled and tested using the same electrolytes. First, half-cell studies were undertaken to determine how

the additive was interacting with the electrodes. As can be seen from the data shown in **Figure 7b**, there was no interaction evident on the cathode. On the anode, increasing concentrations of PzTFE seemed to shift and flatten the decomposition peak of EC at 0.6 V, but no peaks were evident that would indicate a new decomposition product. This information indicates that any effect on the cycling performance could be attributed to interaction with the bulk electrolyte, rather than with cathode/electrolyte and anode/electrolyte interface.

Subsequently, NMC622/graphite full cells were assembled and cycled at 55°C with a 1 C rate for 100 cycles at 55ºC. The capacity, capacity retention and Coulombic efficiency data are shown in **Figure 8**. It is clear that the PzTFE additive cell delivers a much higher capacity retention (80.8%) than the baseline Gen 2 electrolyte cell (64.7%) under the same testing conditions, along with a more consistent Coulombic efficiency. This was compared with other fluorinated ether-substituted derivatives PzTFP and PzHFiP, and while they tended to show favorable performance relative to Gen 2 electrolyte alone, PzTFE was still the overall superior additive.

The improved performance of the phosphazene derivatives are attributed to an *in-situ* interaction with the PF_5 generated under elevated temperatures from the $LiPF_6$ salt. This interaction is weak enough to prevent forming a stable adduct which can unfavorably alter the LiPF6 thermal decomposition equilibrium. However, it is enough to lower the reactivity of PF_5, thus preventing it from reacting further and accelerating the process of electrolyte

degradation. This allows the electrolyte containing the fully substituted phosphazenes to maintain high stability, thus improving cycling performance of the lithium-ion battery under elevated temperature conditions.

4. Conclusions

In this work, a novel NMR setup/method was introduced for observing electrolyte thermal decomposition process. We have verified that it is representative for thermal decay study, and that the effect of electrolyte additives known to suppress decomposition could be directly observed. The NMR method directs the design of a series of substituted phosphazene-based electrolyte additives, which our NMR experiment predicts would act in a similar fashion. The NMC622/graphite cell testing indicates the NMR-guided additive design is beneficial for the cell cycling performance at high temperatures, therefore highlighting the effectiveness of this method.

Acknowledgments

Support from David Howell and Brian Cunningham at Vehicle Technologies Office (VTO), Office of Energy Efficiency and Renewable Energy, U.S. Department of Energy is gratefully acknowledged. NMC622 cathode and graphite anode were fabricated at Argonne's Cell Analysis, Modeling, and Prototyping (CAMP) Facility. Argonne National Laboratory's work was supported by the U.S. Department of Energy, Office of Energy Efficiency and Renewable Energy (EERE), Office of Vehicle Technologies (VTO), Battery Materials Research (BMR) Program, under contract DE-AC02-06CH11357.

References

1. Botte, G. G.; White, R. E.; Zhang, Z., Thermal Stability of $LiPF_6$–EC: EMC Electrolyte for Lithium Ion Batteries. *Journal of Power Sources* **2001**, *97*, 570-575.
2. Chen, Z. H.; Liu, J.; Amine, K., Lithium Difluoro(Oxalato)Borate as Salt for Lithium-Ion Batteries. *Electrochem Solid St* **2007**, *10*, A45-A47.
3. Philippe, B.; Dedryvère, R. m.; Gorgoi, M.; Rensmo, H. k.; Gonbeau, D.; Edström, K., Improved Performances of Nanosilicon Electrodes Using the Salt LiFSI: A Photoelectron Spectroscopy Study. *Journal of the American Chemical Society* **2013**, *135*, 9829-9842.
4. Xu, C.; Jeschull, F.; Brant, W. R.; Brandell, D.; Edstrom, K.; Gustafsson, T., The Role of LiTDI Additive in $LiNi_{1/3}Mn_{1/3}Co_{1/3}O_2$/ Graphite Lithium-Ion Batteries at Elevated Temperatures. *Journal of the Electrochemical Society* **2018**, *165*, A40-A46.
5. Yang, H.; Zhuang, G. V.; Ross, P. N., Thermal Stability of $LiPF_6$ Salt and Li-Ion Battery Electrolytes Containing $LiPF_6$. *Journal of Power Sources* **2006**, *161*, 573-579.
6. Rollins, H. W.; Harrup, M. K.; Dufek, E. J.; Jamison, D. K.; Sazhin, S. V.; Gering, K. L.; Daubaras, D. L., Fluorinated Phosphazene Co-Solvents for Improved Thermal and Safety Performance in Lithium-Ion Battery Electrolytes. *Journal of Power Sources* **2014**, *263*, 66-74.
7. Campion, C. L.; Li, W. T.; Euler, W. B.; Lucht, B. L.; Ravdel, B.; DiCarlo, J. F.; Gitzendanner, R.; Abraham, K. M., Suppression of Toxic Compounds Produced in the Decomposition of Lithium-Ion Battery Electrolytes. *Electrochem Solid St* **2004**, *7*, A194-A197.
8. Hall, D. S.; Hynes, T.; Dahn, J. R., Dioxazolone and Nitrile Sulfite Electrolyte Additives for Lithium-Ion Cells. *Journal of the Electrochemical Society* **2018**, *165*, A2961-A2967.
9. Han, Y.-K.; Yoo, J.; Yim, T., Why Is Tris(Trimethylsilyl) Phosphite Effective as an Additive for High-Voltage Lithium-Ion Batteries? *Journal of Materials Chemistry A* **2015**, *3*, 10900-10909.
10. Harrup, M. K.; Gering, K. L.; Rollins, H. W.; Sazhin, S. V.; Benson, M. T.; Jamison, D. K.; Michelbacher, C. J.; Luther, T. A., Phosphazene Based Additives for Improvement of Safety and Battery Lifetimes in Lithium-Ion Batteries. *ECS Transactions* **2012**, *41*, 13-25.
11. Kang, K. S.; Choi, S.; Song, J.; Woo, S. G.; Jo, Y. N.; Choi, J.; Yim, T.; Yu, J. S.; Kim, Y. J., Effect of Additives on Electrochemical Performance of Lithium Nickel Cobalt Manganese Oxide at High Temperature. *Journal of Power Sources* **2014**, *253*, 48-54.
12. Kim, G. Y.; Dahn, J. R., The Effect of Some Nitriles as Electrolyte Additives in Li-Ion Batteries. *Journal of the Electrochemical Society* **2015**, *162*, A437-A447.
13. Li, W. T.; Campion, C.; Lucht, B. L.; Ravdel, B.; DiCarlo, J.; Abraham, K. M., Additives for Stabilizing $LiPF_6$-Based Electrolytes against Thermal Decomposition. *Journal of the Electrochemical Society* **2005**, *152*, A1361-A1365.
14. Lin, Y. C.; Zhang, H.; Yue, X. P.; Yu, L.; Fan, W. Z., Triallyl Phosphite as an Electrolyte Additive to Improve Performance at Elevated Temperature of $LiNi_{0.6}Co_{0.2}Mn_{0.2}O_2$/Graphite Cells. *Journal of Electroanalytical Chemistry* **2019**, *832*, 408-416.
15. Smart, M. C.; Lucht, B. L.; Ratnakumar, B. V., The Use of Electrolyte Additives to Improve the High Temperature Resilience of Li-Ion Cells. *ECS Transactions* **2008**, *11*, 79-89.

16. Sun, X.; Lee, H. S.; Yang, X. Q.; McBreen, J., Using a Boron-Based Anion Receptor Additive to Improve the Thermal Stability of $LiPF_6$-Based Electrolyte for Lithium Batteries. *Electrochemical and Solid-State Letters* **2002**, *5*.
17. Zhang, S. S.; Xu, K.; Jow, T. R., A Thermal Stabilizer for $LiPF_6$-Based Electrolytes of Li-Ion Cells. *Electrochemical and solid-state letters* **2002**, *5*, A206-A208.
18. Xu, C.; Renault, S. v.; Ebadi, M.; Wang, Z.; Björklund, E.; Guyomard, D.; Brandell, D.; Edstrom, K.; Gustafsson, T., Litdi: A Highly Efficient Additive for Electrolyte Stabilization in Lithium-Ion Batteries. *Chemistry of Materials* **2017**, *29*, 2254-2263.
19. Ravdel, B.; Abraham, K. M.; Gitzendanner, R.; DiCarlo, J.; Lucht, B.; Campion, C., Thermal Stability of Lithium-Ion Battery Electrolytes. *Journal of Power Sources* **2003**, *119*, 805-810.
20. Campion, C. L.; Li, W. T.; Lucht, B. L., Thermal Decomposition of $LiPF_6$-Based Electrolytes for Lithium-Ion Batteries. *Journal of the Electrochemical Society* **2005**, *152*, A2327-A2334.
21. Handel, P.; Fauler, G.; Kapper, K.; Schmuck, M.; Stangl, C.; Fischer, R.; Uhlig, F.; Koller, S., Thermal Aging of Electrolytes Used in Lithium-Ion Batteries – an Investigation of the Impact of Protic Impurities and Different Housing Materials. *Journal of Power Sources* **2014**, *267*, 255-259.
22. Wiemers-Meyer, S.; Winter, M.; Nowak, S., Mechanistic Insights into Lithium Ion Battery Electrolyte Degradation–a Quantitative NMR Study. *Physical Chemistry Chemical Physics* **2016**, *18*, 26595-26601.
23. Grutzke, M.; Weber, W.; Winter, M.; Nowak, S., Structure Determination of Organic Aging Products in Lithium-Ion Battery Electrolytes with Gas Chromatography Chemical Ionization Mass Spectrometry (GC-CI-MS). *Rsc Advances* **2016**, *6*, S7253-S7260.
24. Wiemers-Meyer, S.; Winter, M.; Nowak, S., A Battery Cell for in Situ NMR Measurements of Liquid Electrolytes. *Phys Chem Chem Phys* **2017**, *19*, 4962-4966.
25. Yin, S. C.; Rho, Y. H.; Swainson, I.; Nazar, L. F., X-Ray/Neutron Diffraction and Electrochemical Studies of Lithium De/Re-Intercalation in $Li_{1-X}Co_{1/3}Ni_{1/3}Mn_{1/3}O_2$ (X= 0→1). *Chemistry of materials* **2006**, *18*, 1901-1910.
26. Liu, J., et al., Fluorinated Phosphazene Derivative – a Promising Electrolyte Additive for High Voltage Lithium Ion Batteries: From Electrochemical Performance to Corrosion Mechanism. *Nano Energy* **2018**, *46*, 404-414.
27. Zhang, Q.; Noguchi, H.; Wang, H. Y.; Yoshio, M.; Otsuki, M.; Ogino, T., Improved Thermal Stability of $LiCoO_2$ by Cyclotriphosphazene Additives in Lithium-Ion Batteries. *Chemistry Letters* **2005**, *34*, 1012-1013.

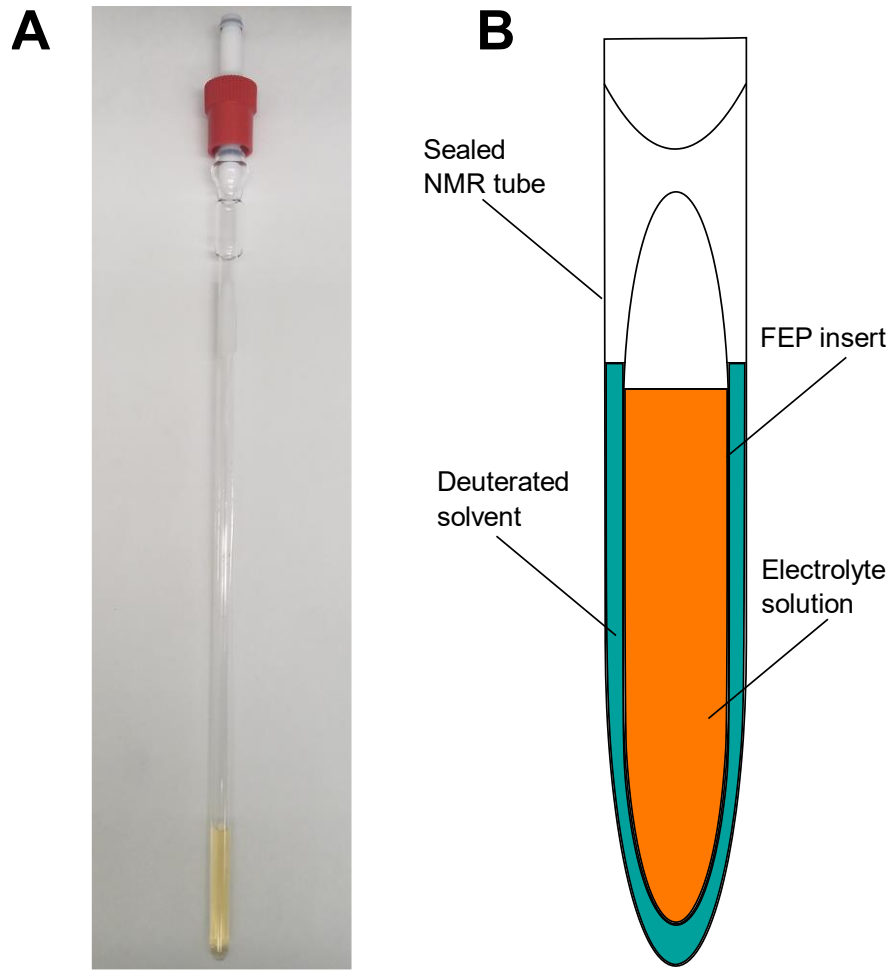

Figure 1. NMR experimental setup. (a) Picture of NMR tube with an PTFE/FEP insertion and (b) schematics of the NMR setup.

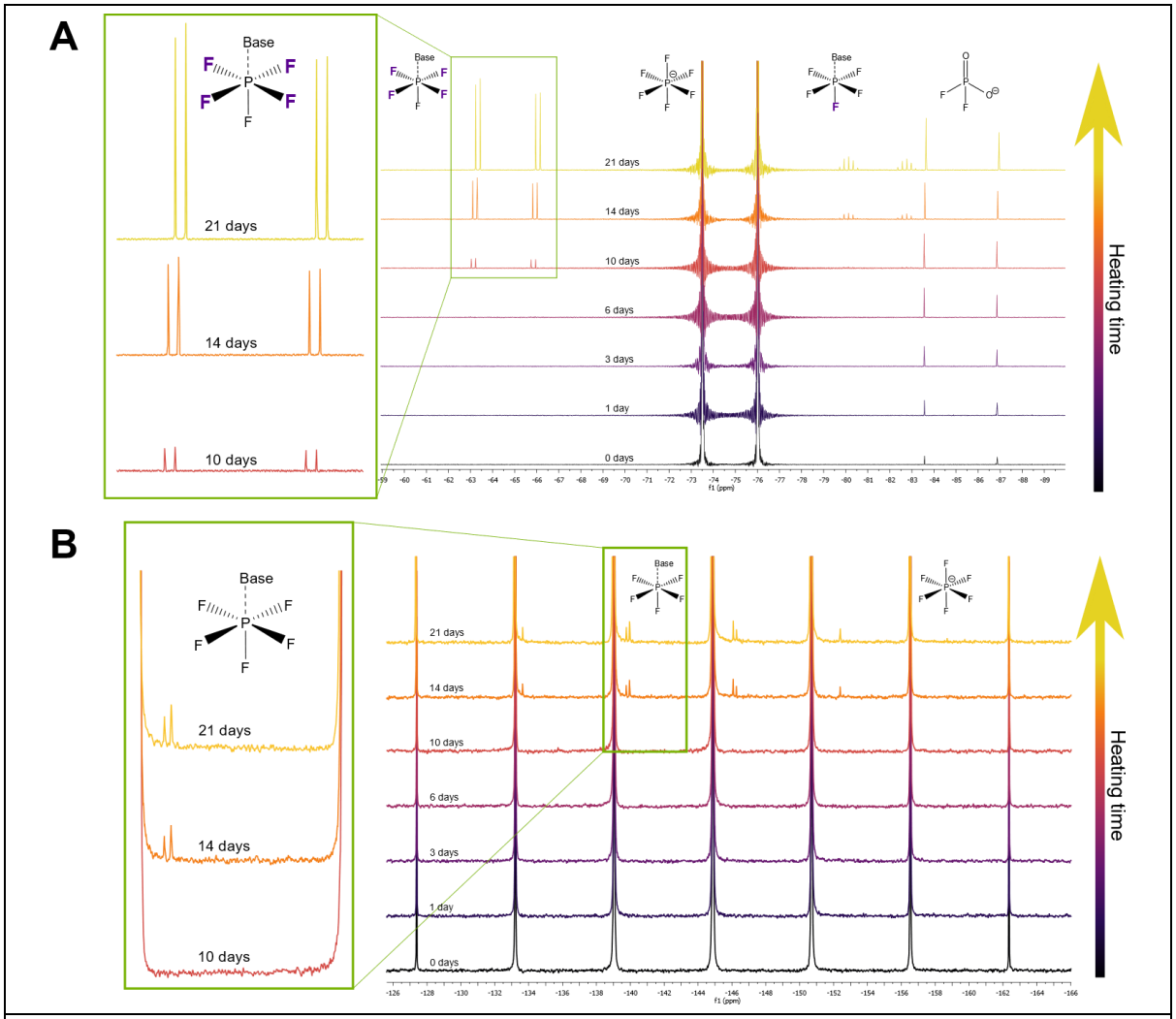

Figure 2. (a) ^{19}F NMR and (b) ^{31}P NMR spectra of Gen 2 electrolyte heated at 80°C for increasing lengths of time.

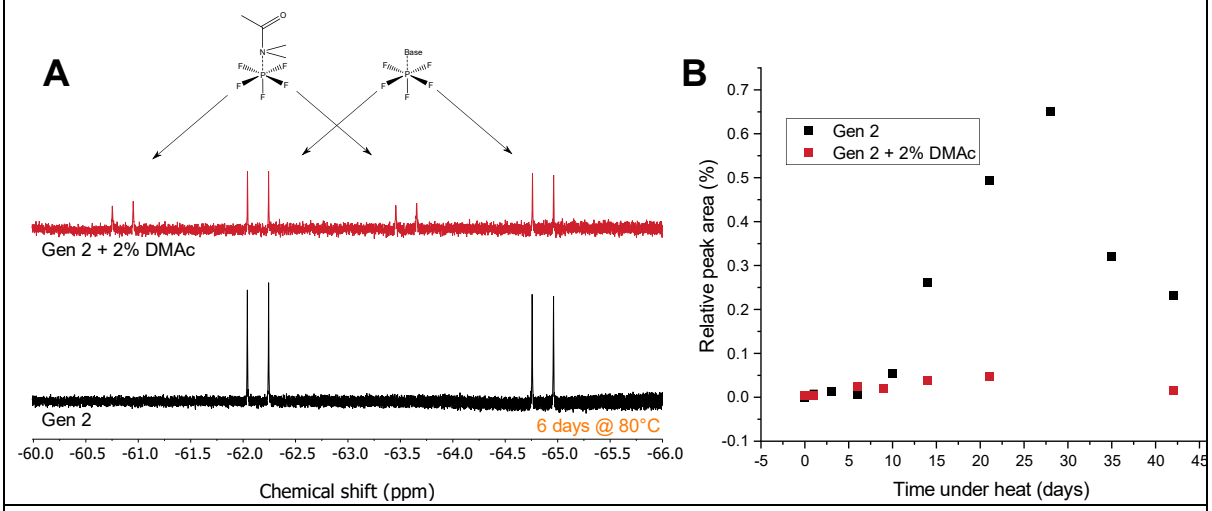

Figure 3. (a) ^{19}F NMR spectra of Gen 2 with DMAc (top) and Gen 2 (bottom) after 6 days of heating at 80°C, and (b) peak area of PF_5 complex signals relative to $LiPF_6$ salt in the solution.

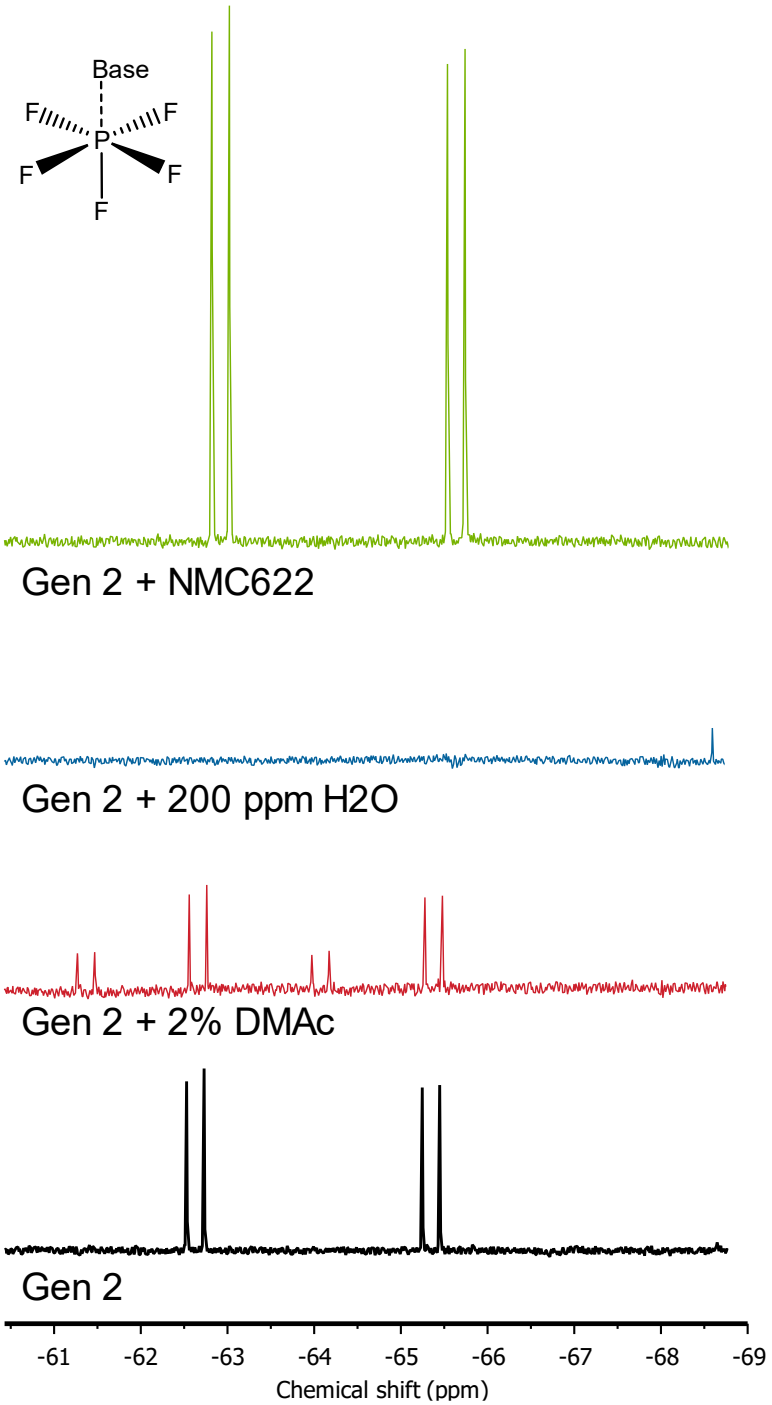

Figure 4. ^{19}F NMR spectra after aging at elevated temperatures from bottom to top: Gen 2 @ 80°C, Gen 2 + 2% DMAc @ 80°C, Gen 2 + 200 ppm H_2O @ 50°C, and Gen 2 + NMC powder @ 50°C.

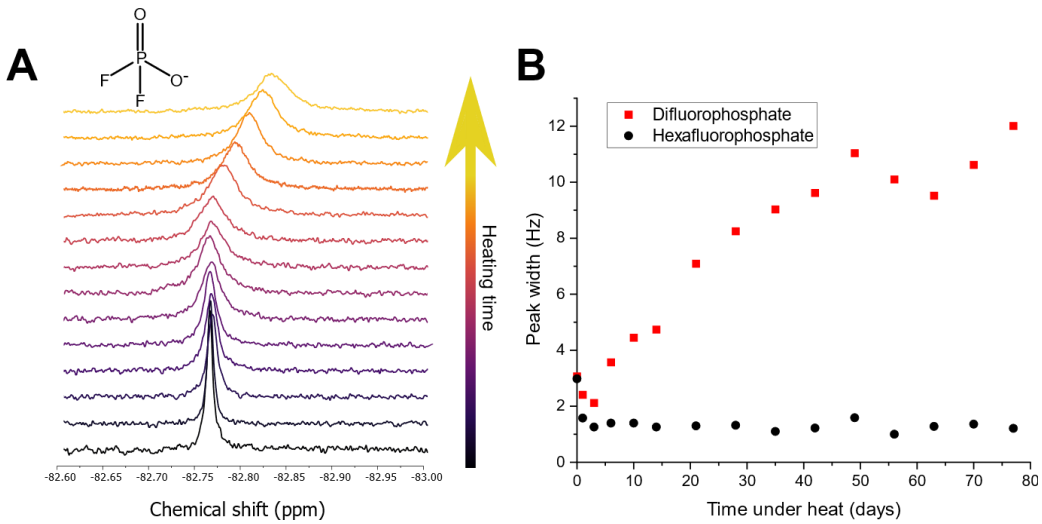

Figure 5. (a) ^{19}F NMR spectra of Gen 2 + NMC powder after being heated for various days, and (b) peak widths for different signals *vs* heating time.

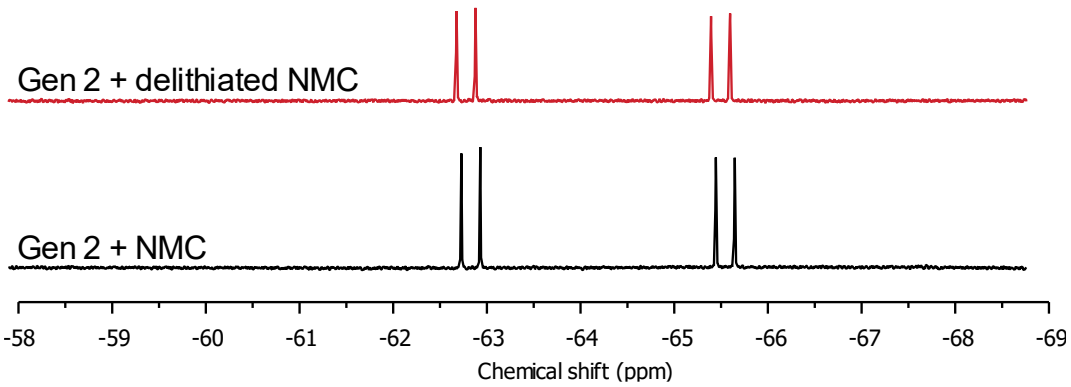

Figure 6. ^{19}F NMR spectra after aging of NMC powder (top) and delithiated NMC powder (bottom) in Gen 2 electrolyte.

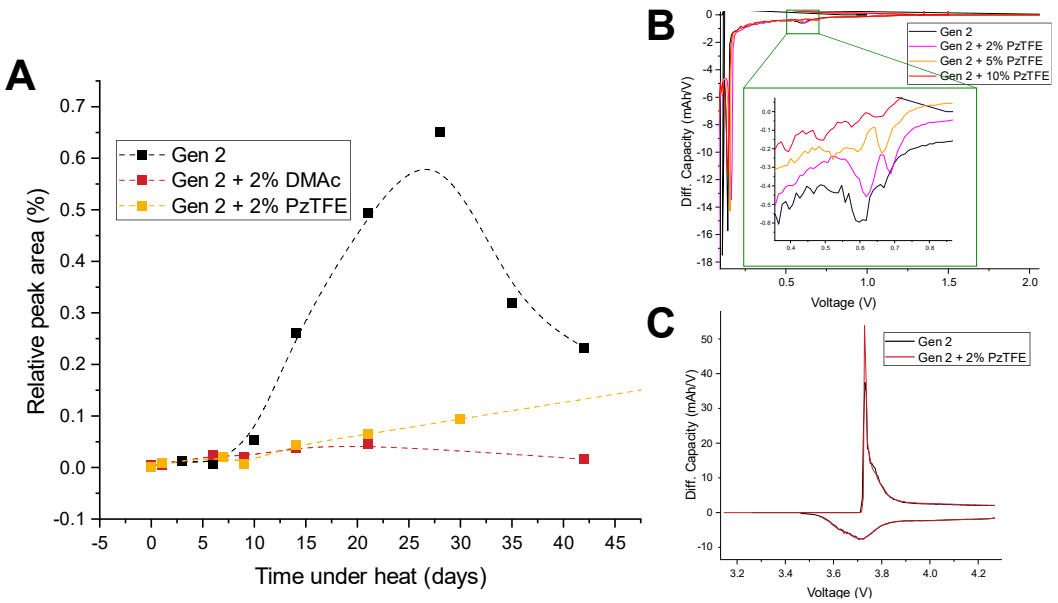

Figure 7. (a) ^{19}F NMR peak area of PF_5 complex signals relative to $LiPF_6$, and differential capacity profiles (*dQ*/*dV*) of the 1st cycle of (b) graphite/Li half-cells and (c) NMC622/Li half-cells with increasing concentrations of PzTFE additive.

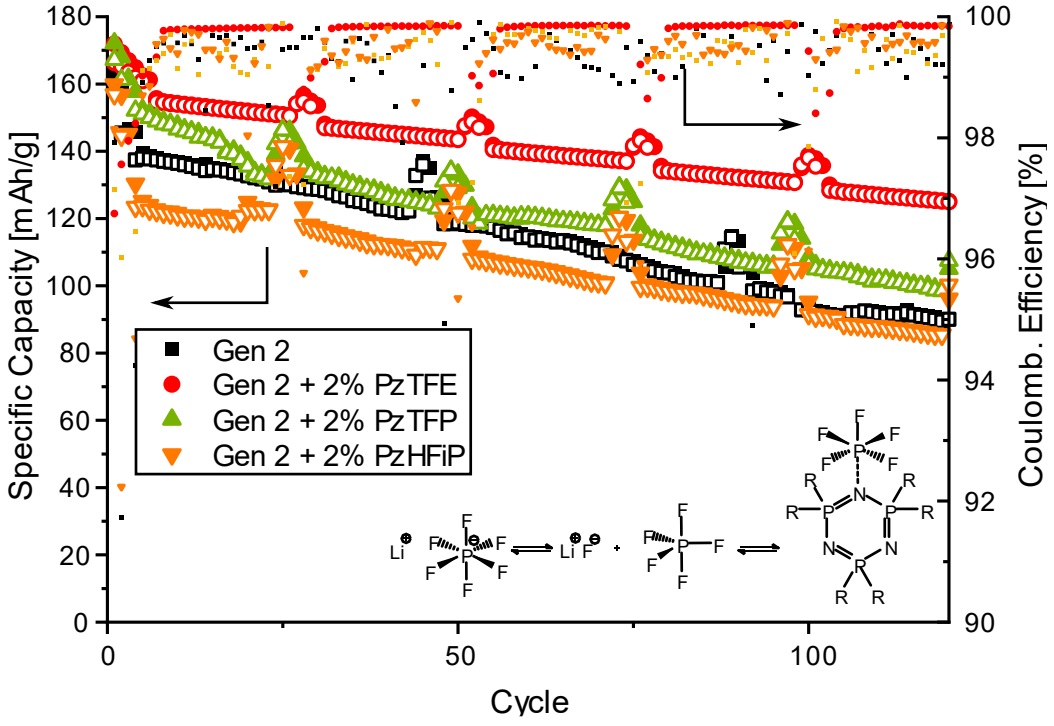

Figure 8. Specific capacity and Coulombic efficiency of NMC622/graphite cells with various electrolytes containing 2% PzTFE, 2% PzTFP, and 2% PzHFiP as well as Gen 2 electrolyte alone cycled at 55°C.

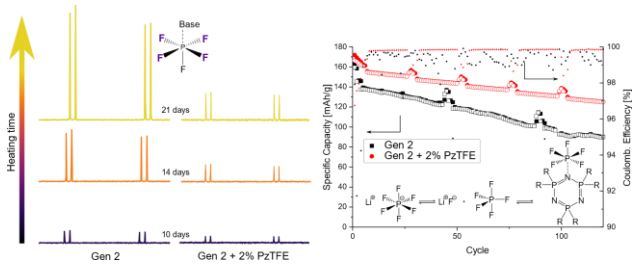
Base
21 days
14 days
10 days
Heating time
Gen 2
Gen 2 + 2% PzTFE

Specific Capacity [mAh/g]
Coulomb. Efficiency [%]
Cycle
Gen 2
Gen 2 + 2% PzTFE

TOC Graphic